Indonesian Journal of Aerospace Vol. 21 No. 1 Juni 2023 : pp 25 – 38 (Dinaryanto et al.)
DOI: 10.59981/ijoa.2023.116
https://ejournal.brin.go.id/ijoa/

An Integrated Numerical Investigation on the Aerodynamic Characteristics and Vortex Development of Airfoil Using Spalart-Allmaras Model

Okto Dinaryanto[1*] , Bahrul Jalaali[1], Muhammad Hisyam[1], Teguh Wibowo[1]

[1]*Department of Mechanical Engineering, Faculty of Aerospace Technology, Institut Teknologi Dirgantara Adisutjipto, Blok R Lanud. Adisutjipto, Yogyakarta 55198, Indonesia*

*Corresponding e-mail: okto.dinaryanto@itda.ac.id

Received: 19-01-2023. Accepted: 11-5-2023. Published: ..... (DDMMYYY)

Abstract

In this paper, airfoils' computational fluid dynamics study assessed aerodynamic characteristics and vortex development by varying the angle of attack (α) and flap deflection angles. The flow characteristics over three airfoil models (NACA0021, NACA2409, NACA2409+Fowler flap) were numerically simulated. The approach of the finite volume model was employed to solve the mass and momentum governing equation. The reliable Spalart-Allmaras (S-A) turbulent model was used and validated using reported data from the experiment in terms of lift and drag coefficients. The numerical simulation successfully obtained good results in analyzing fluid flow over the airfoil. Detailed explanations of simulation steps were also presented. The vortex development and air separation were clearly captured. The results of the symmetric airfoil showed that the vortex shedding regimes occurred at α = 8°, and the critical stall angle was about 14°. The value was higher for the NACA2409, where the airflow exhibited a relatively more stable behavior. Moreover, it is evident that flap addition altered lift-drag characteristics. The value of the lift-to-drag ratio increased due to the increase of C_l. The parametric study was done on the α and flap deflection angle to attain the desirable airfoil configuration. The maximum result of airfoil configuration was obtained on the NACA2409 at α = 12° with 10^0 flap deflection angles while it enhanced the lift coefficient by about 54%. This study is beneficial for initial aircraft design on the aerodynamics aspect of an airfoil and a wing analysis.

Keywords**:** *Aerodynamics; CFD; Spalart-Allmaras; Turbulent.*

1. Introduction

Aerodynamics analysis deals with the interaction of air on moving bodies. The study is significant in designing commercial products such as aircraft (Torres et al., 2001, Kay et al., 2020) and viable wind turbines (Rocha et al., 2016, Shukla and Kaviti., 2017, Crivellini et al., 2014). In aerodynamics analysis, understanding airfoil performance becomes the fundamental yet important aspect of the study. In this regard, the basic shape of the airfoil may vary based on its main application. For instance, a symmetric airfoil is generally used for empennage, while the non-symmetric one is employed to generate lift on an aircraft wing (Ahmed et al., 2005). A comprehensive understanding of airfoil characteristics is very beneficial as an initial step before extending the field of analysis into a three-dimensional framework (i.e., wing aerodynamics analysis). Generally, the analysis can be performed in three methods, i.e., analytical solution, experimental, and numerical approximation. Notably, an analytical solution is mainly beneficial when solving certain basic and simple problems. However, the experiment is often costly and hard to conduct (Anderson and Wendt., 2008).

Furthermore, experiments may not be able to provide the sets of data needed for achieving a reliable design (Wolfe and Ochs., 1997). Numerical simulation of aerodynamics can be a promising tool to overcome the aforementioned. In the early

1970s, a numerical simulation based on Reynolds-averaged Navier-Stokes (RANS) was performed by NASA (Wendt., 2008). The analysis indicated a concerning problem in the airflow towards bodies involving turbulence phenomena

Previously, both experimental and numerical studies had been performed accordingly. Aerodynamics assessment on an airfoil was performed by an experimental test as reported in previous research. The studies found that the airfoil flow characteristic was typically obtained as pressure and velocity distribution and lift-drag characteristics. In order to reduce the experimental test cost and time, a numerical investigation is prior needed to be done. Computational fluid dynamics (CFD) analysis has been widely carried out to observe the aerodynamics characteristics (Windte et al., 2006), (Crivellini et al., 2014), (Rao et al., 2018) and (Li et al., 2002) found that increase in lift-to-drag coefficient was related to the flap addition. A similar trend was also found (Rhee et al. 2003) towards hydrofoil and (Roztamzadeh et al. 2013) on the undulated airfoil. However, those works did not reveal the detailed steps of the simulation as well as the particular numerical consideration. The Spalart-Allmaras (S-A) equation-based model for transitional flows has been widely used for aerospace applications, as reported by Refs. (Spalart and Allmaras, 1994), (Andrea et al., 2013), (Shukla and Kaviti., 2017), and (Crivellini et al., 2014). The model was reliable on several aerodynamic characteristics and exhibited a quite stable and good numerical convergence. The S-A model calculates a transport equation for kinematic viscosity, while it does not consider the calculation of length scale related to the shear layer thickness (ANSYS Theory guide, 2016).

Based on preceding studies showed that CFD was a powerful tool for investigating physical aerodynamic phenomena. However, only limited studies focus on clear explanations in the aerodynamics simulation of the airfoil, and this work aims to fill the previously mentioned gaps. A brief description of this work is given in the following points. First, this study aims to present the best practice of CFD analysis in investigating aerodynamic characteristics. It intends to advise on achieving high-quality CFD simulation using the S-A equation. Second, the S-A turbulent model is then used to observe the aerodynamic characteristics and obtain the desired numerical accuracy. Third, numerical validation is presented by comparing the simulation results with those obtained by the experimental result obtained from the wind tunnel section. Fourth, a numerical investigation of flap addition on the airfoil towards lift-drag behavior is given. This study adopts three airfoil models; NACA 0021, NACA 2409, and NACA 2409+ Fowler flap. The variations of the angle of attack (α) and flap deflection angle are performed to assess the aerodynamic characteristics. In addition, this study will hopefully enrich the reference for data-driven turbulence modeling for aerodynamics analysis (Duraisamy et al., 2019, Brunton, S.L. 2022).

2. Methodology

2.1. Modelling and Problem Formulation

In the present work, we will profoundly discuss the investigation of the airfoil characteristic towards the aerodynamics characteristic. Numerical modeling was carried out using a two-dimensional (2D) domain. The geometry of NACA 0021 and NACA 2409 was used based on the open-source data on the 4-digit NACA database (Airfoiltools, (2021)). We add the Fowler flap to the airfoil model to present the reliability of the current CFD model for analyzing airfoil with flap. The airfoil models used in this work illustrate in Figure. 1, where Figure. 1 (a) is the profile of a symmetrical airfoil, Figures. 1 (b) and (c) represent standard NACA 2409 and its Fowler-flapped configuration with 20° flap deflection shows. The chord flap (cf), overlap, and flap gap are determined as follows: , $cf = 0.4c$ $overlap = 1.5\%c$ and $flap\ gap = 2.7\%c$, whereby the airfoil chord (c) is 1000mm.

(a) (b) (c)

Figure 1. Airfoil model for (a) NACA 0021 (b) NACA 2409 (c) NACA 2409 + Fowler flap.

The mathematical formulation of the fluid analysis is carried out by using governing equations of mass and transport. The governing equations are presented in terms of the continuity equation for mass balance, momentum equation, and Spalart Allmaras (S-A) for analyzing the turbulence model while the RANS model is utilized. This step was done by determining the simulation parameters, such as; the airflow velocity, solid surface geometry, wall function, drag force, and flow regime. The known turbulence modeling constant values are obtained (ANSYS theory guide, 2016). The variable considered in the S-A model is the turbulent viscosity ($\tilde{v}$). It is in accordance with the regions which are not affected by a strong viscous effect. The transport equation of S-A consists of the production, source, and destruction term. We provide the S-A model reported in Refs. (Spalart and Allmaras 1994), (ANSYS Theory guide, 2016), and (Shukla and Kaviti. (2017), which is applicable to the free shear flows and can treat turbulent flow over a body (Eq.2-1). In addition, it also provided relatively good results when it deals with aerodynamic phenomena. In Eq. 2-1, G_T , Y_v and $S_{\tilde{v}}$ are the production and destruction of turbulent viscosity and source term while $\widetilde{\sigma_v}$ and C_{b2} are the constant (ANSYS Theory guide, 2016). The related variable is described in Eqs.2-2 – 2-6. While the nomenclatures and constans are provided in Table 2-1 and 2-2, respectively. On applying the method, we organize the effects of initial and boundary conditions. No universally general turbulence model is accurate for all kinds of flows. Hence, this work is proposed to figure out the suitable S-A turbulent model for a particular case. Parametric studies investigate the influence of the angle of attack and flap deflection on the aerodynamic characteristics. The angle of attack (α) is defined as the angle between incoming air and the relative wind with respect to the airfoil reference line (Shukla and Kaviti, 2017). Here, the α variations are modified in the range of 0°-14°. Meanwhile, the flap deflection angle of the 2409+flap model is adjusted to 10°-30°.

$$\frac{D\tilde{v}}{Dt} = G_v - Y_v + \frac{1}{\widetilde{\sigma_v}}[\nabla.\{(v+\tilde{v})\nabla\tilde{v}\} + C_{b2}(\nabla\tilde{v})^2] + S_{\tilde{v}} \quad (2\text{-}1)$$

$$G_v = C_{b1}\rho\left(S + \frac{\tilde{v}}{\kappa^2 d^3}\left(1 - \frac{\chi}{1+\chi f_{v1}}\right)\right)\tilde{v}\,;\ \chi = \frac{\tilde{v}}{v} \quad (2\text{-}2)$$

$$Y_v = \left(\frac{C_{b1}}{\kappa^2} + \frac{(1+C_{b2})}{\widetilde{\sigma_v}}\right)\rho g_t\left[\frac{1+{C_{w3}}^6}{{g_t}^6+{C_{w3}}^6}\right]^{\frac{1}{6}}\left(\frac{\tilde{v}}{d}\right)^2 \quad (2\text{-}3)$$

$$S = \sqrt{2(\frac{1}{2}(\frac{\partial \boldsymbol{u}_i}{\partial x_j} - \frac{\partial \boldsymbol{u}_j}{\partial x_i}))(\frac{1}{2}\left(\frac{\partial \boldsymbol{u}_i}{\partial x_j} - \frac{\partial \boldsymbol{u}_j}{\partial x_i}\right))} \quad (2\text{-}4)$$

$$g_t = \left(\zeta + C_{w2}(\zeta^6 - \zeta)\right) \quad (2\text{-}5)$$

$$\zeta = \tilde{v}/\left[\left(S + \frac{\tilde{v}}{\kappa^2 d^3}\left(1 - \frac{\chi}{1+\chi f_{v1}}\right)\right)\kappa^2 d^2\right] \quad (2\text{-}6)$$

Table 2-1. Nomenclatures

Symbol	Nomenclature	Unit
ρ	Density of fluid	kg/m^3
P	Pressure	Pa
g	Gravitational acceleration	m/s^2
μ	Dynamic viscosity	kg/m-s

V	Velocity vector	m/s
υ	Kinematic viscosity	m^2/s
$\tilde{\upsilon}$	Turbulent kinematic viscosity	m^2/s
S	Scalar measure of deformation tensor	m
d	Distance from the wall	m
S_v	Source term	m^2/s
Y_v	Destruction of turbulent viscosity	m^2/s
G_T	Production of turbulent viscosity	m^2/s
S	The magnitude of the vorticity	m^2/s

Table 2.2 Model constants

Constant	Value
C_{b1}	0.1355
C_{b2}	0.622
$\widetilde{\sigma_v}$	0.667
$C_{v1}C_{v1}$	7.1
$C_{w2}C_{w2}$	0.3
$C_{w3}C_{w3}$	2.0
$\kappa\kappa$	0.4187

2.2. Computational setup

The meshing process was very carefully handled by using unstructured mesh. It is crucial as poor simulation results may arise due to a lack of convergence and discretization methods (Andersson et al., 2011). The mesh variations are generated for different parts in the domain, such as between the outer main domains, the mesh control domain, and the airfoil. In order to enhance the numerical accuracy and computational efficiency, the grid refinement technique was adopted. The numerical error can be reduced by utilizing finer grid resolution (Casey and Wintergerste, 2000). Both mesh quality and aspect ratio were modified to be less than 0.8 and 0.7, respectively. Besides, the mesh skewness was altered below 0.85. The mesh thickness was composed smaller on the airfoil body using the inflation method (Figure. 2-1 (a)). The purposes were to accurately capture the boundary layer, separate the airfoil profile from the outer domain, and observe the effect of air at the airfoil edge. Whereby the effect of the flap was considered by increasing the number of elements over the flap body. The high fine mesh was used, while the span angle center and smoothing effect were taken with the high and fine setting. To observe the effect of wind over the airfoil body, we consider a sufficient area of domain. An atmospheric setup was made, whereas the airfoil was designed at the center of a domain alongside the boundary condition. The domain is illustrated in Figure. 2-1(b), where A and B, and C denote the length of the domain, which, in this study, is defined as $A = 10c$ and $B = 20c$.

A complementary CFD investigation was done using ANSYS-Fluent Academic. In the solver step, boundary conditions and input parameters were defined. The air velocity was set to 80 m/s while Reynolds number was $5\,x\,10^6$. Numerical discretization was implemented while steady-state and pressure-based solvers were set. The viscous S-A model was utilized with vorticity-based and curvature correction addition, and the value of correction remained constant by 1. Some employed assumptions were: fluid as an ideal gas, no heat transfer process, and the airflow determined at the subsonic domain. The no-slip wall boundary condition was applied at the surface of the airfoil. At the inlet, the turbulence properties were set to a turbulence intensity of 5%, and the zero pressure and uniform velocity were set. The fixed pressure value and zero velocity gradient were chosen at the outlet, and open boundary conditions were applied to the top and bottom of the wall domain. The solution method Pressure-Velocity coupling, was used with a coupled method on the second-order spatial discretization. Moreover, we first focussed on the standard airfoil to perform the lift and drag aerodynamics analysis. The results were then validated towards the experimental results. Next, we applied the flap addition to testing the current method to analyze more complex shapes. The parametric study was done on the various airfoil and flap orientations

by taking into account the α and flap deflection.

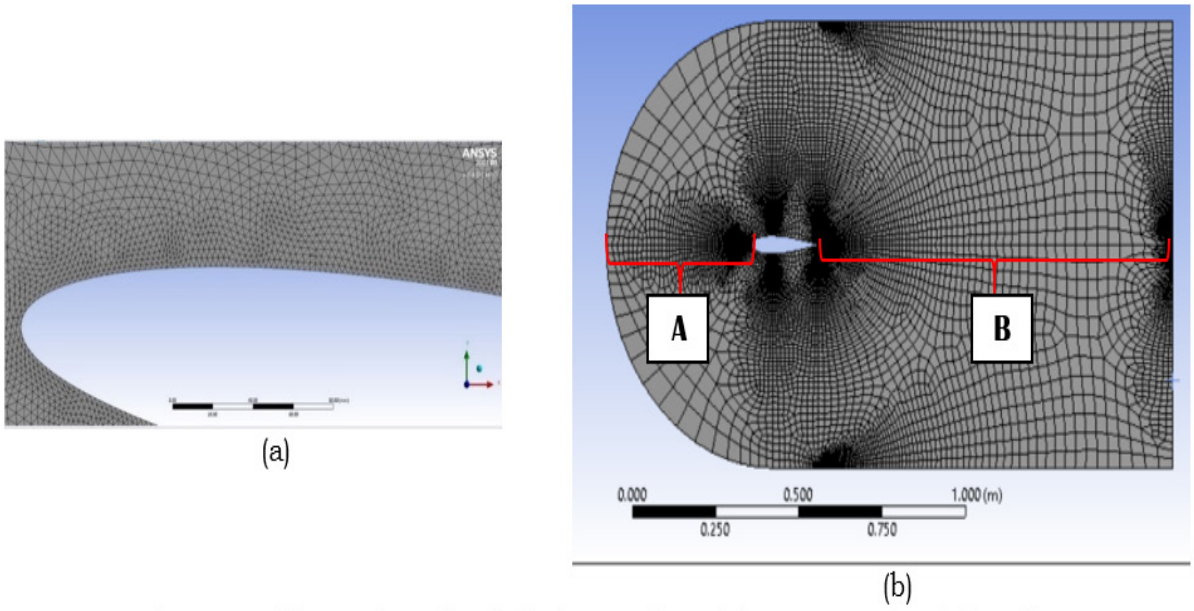

Figure 2-1. illustration of (a) inflation mesh and (b) computational domain

3. Result and Analysis

3.1. Grid Independence Test and Validation

In our simulation, a strictly developed unstructured mesh for the model and flow domain was chosen and determined as an adequate model. The grid independence test was first carried out with mesh numbers of 106,848, 87,381, and 80,451 elements. The test aimed to show the grid-independent solution whereby the calculation and results will not change when refined (Casey and Wintergerste, 2000). The lift and drag coefficients (C_l, C_d) will be observed as reference values. The reference values of C_l and C_d at α = 6° from the experimental results (Gregorek et al., 1989) were 0.528 and 0.011, respectively. The simulation was based on a 1.2 Mach velocity inlet using NACA 0021. The selected test runs and the number of elements are summarized in Table 3-1. Here, the result reveals only a small difference in lift and drag coefficients value while increasing the number of elements. Moreover, this then can be expressed that only a slight difference from obtained simulation results towards the actual experimental result reported (Gregorek et al., 1989). Despite a slight overestimation of C_d value, the overall agreements between these results and those from the literature (Gregorek et al., 1989) are considered satisfactory. Hence, the remaining simulation will use Case B of 87,381 elements.

Table 3-1. Grid independence study and validation

Case	Number of Element	C_l	Difference (%)	C_d	Difference (%)
Experiment	-	0.528		0.011	
A	80,451	0.564	6.84	0.013	16.83
B	87,381	0.564	6.84	0.013	16.83
C	106,848	0.563	6.72	0.013	16.83

3.2. Aerodynamics Characteristic

The coefficient of lift and drag are defined as follows: $C_d = \frac{F_d}{\frac{1}{2}\rho_0 {u_0}^2 C}$ and $C_l = \frac{F_l}{\frac{1}{2}\rho_0 {u_0}^2 C}$. Whereby 0 denotes the condition of far-field, F_d and F_l are the drag and lift force. u represents the relative flow velocity to the object. The value of C_l and C_d measure the efficiency and the performance of an airfoil. This analysis is useful then for further wing inspection and design. The flap addition has its advantages towards lift enhancement, as discussed later. In aircraft analysis, the increased lift and reduced drag give much higher efficiency. It reduces fuel consumption and increases the flight range (Rocha et al., 2016). However, the aerodynamic performances are constrained by the airworthiness requirements such as Part 25 of the Federal Airworthiness Requirement (FAR). Among those requirements, it is enforced to investigate lift and drag characteristics deeper.

For the case of NACA 0021, simulation results (Figures. 3-1(a) and (b)) are shown the velocity and pressure contour for a particular airfoil angle of attack. The velocity and pressure contour is shown in good agreement, as stated in Bernoulli's velocity pressure. From the result, it was found that for $\alpha\alpha$ below 8°, no vortex was observed. The vortex emerged at $\alpha\alpha$ higher than 10° and showed an instantaneous streamline pattern (Figure 3-1(c)). We note that at $\alpha\alpha$ = 8° vortex began to occur at the airfoil tail. As the $\alpha\alpha$ increased, a large-scale air vortex on the airfoil surface became highly unsteady. Moreover, an airflow separation occurs at $\alpha\alpha$ = 13° (Figure 3-1(d)). From the simulation, it is suggested that airfoil orientation has a significant impact on the wing's overall flow and force characteristics.

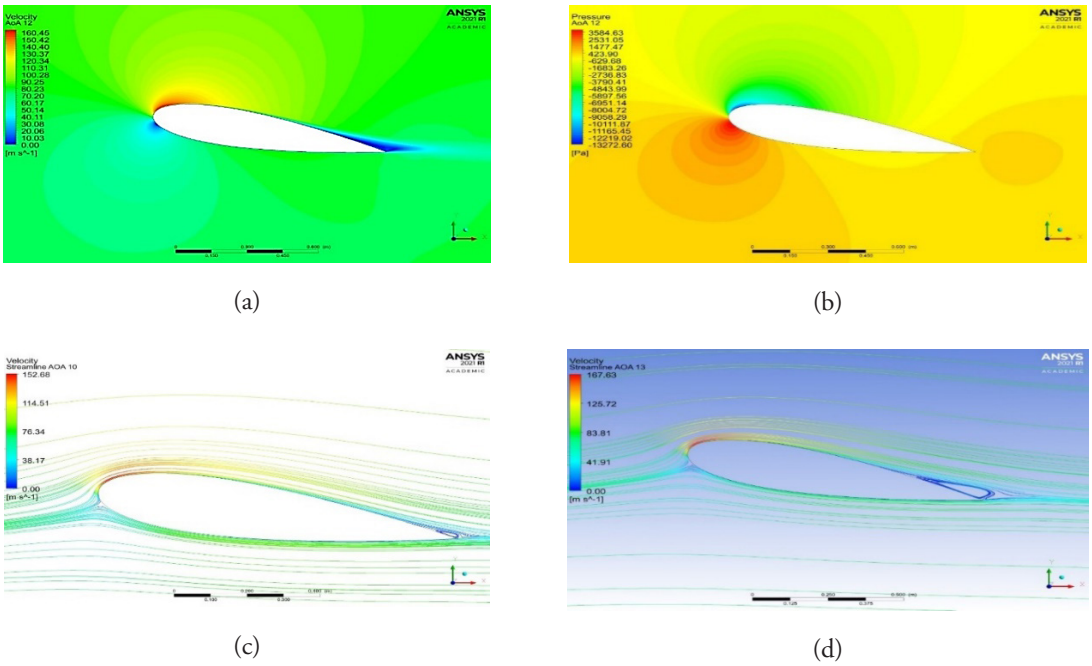

Figure 3-1. Simulation result of NACA 0021. (a) velocity profile at α = 12° (b) pressure contour at α = 12° (c) streamline at α = 10° (d) streamline at α = 13°

Figures. 3-2(a) and (b) illustrated the velocity and contour of NACA2409 airfoil at particular α. The velocity and pressure field results were in line with the physical theory, making it evident that numerical results agreed with the actual phenomena. It was exposed that at α lower than 4°, no flow separation emerged was noticed. The flow separation occurred at a lower α than the NACA0021 airfoil. The recirculation region arose at the airfoil tail, and unsteady vortex shedding was observed at α about 12° (Figure. 3-2(c)). A further increase of α, influenced the airfoil-tail vortex and flowed instability to become larger. We noted that flow separation was observed at α = 14°(Figure 3-2(d)). As the α increases, the flow separation on the airfoil surface takes place and becomes unsteady, leading to the stall condition. However, compared to the symmetrical airfoil, the flow around the airfoil of

NACA2409 is more stable, influencing the higher lift coefficient. Furthermore, the value of C_lC_l vs C_dC_d of NACA0021 and NACA2409 are shown in Figure. 3-3(a). It found that at the same $\alpha\alpha$, on NACA2409 was higher than 0021 by about 10.5%. In addition, the maximum lift of NACA2409 attained in the lower $\alpha\alpha$. Therefore, it was observed that NACA2409 gave more suitable characteristics in terms of aircraft wings, which was useful for decreasing the airborne distance (Wang et al., 2015). The next section investigates the effect of high lift device addition by adding the Fowler flap in NACA2409. The $\alpha\alpha$ 12° was chosen due to the higher value of lift to drag ratio on NACA2409. The optimal flap deflection angle will be observed as well.

To begin with, the aerodynamics analysis of airfoil and high-lift devices merely represents the characteristic of the airfoil, which is then intended to be an initial reference for wing analysis purposes. In this work, the optimum flap deflection angle was evaluated at $\alpha\alpha$ = 12^0 where the maximum value of the NACA2409 lift coefficient was noted. NACA 2409 was chosen in the analysis over standard symmetrical airfoil because it is commonly used in wing configuration. Figure. 3-3 (b) compares the lift-to-drag ratios and lift-drag coefficient with respect to the airfoil flap orientation. The 'none' terms refer to the NACA2409 without flap attached (undeployed). Here, the analysis was based on the optimum value of the lift-drag coefficient ratio. Based on the simulation result, the highest C_lC_l value was encountered on 25° flap deflection by 1.99, while the C_dC_d obtained by 0.46. On the other hand, the value of C_lC_l and C_dC_d in 10° configuration were 1.99 and 0.24, whereby yielded a higher lift-drag ratio. On that account, the highest value of the drag-lift ratio was obtained at 10°. Adding a flap at 10o deflection increases the lift coefficient by about 54% more than the standard configuration.

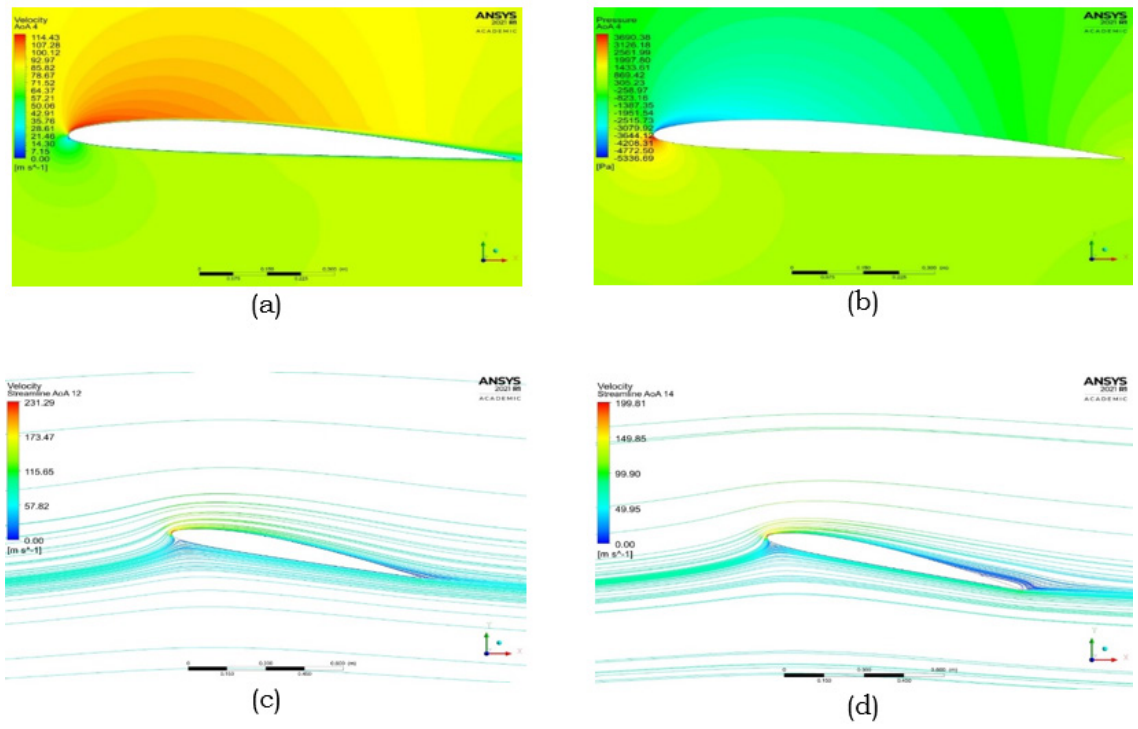

Figure 3-2. Simulation result of NACA 2409. (a) velocity profile at α = 4° (b) pressure contour at α = 4° (b) streamline at α = 12° (d) streamline at α = 14°

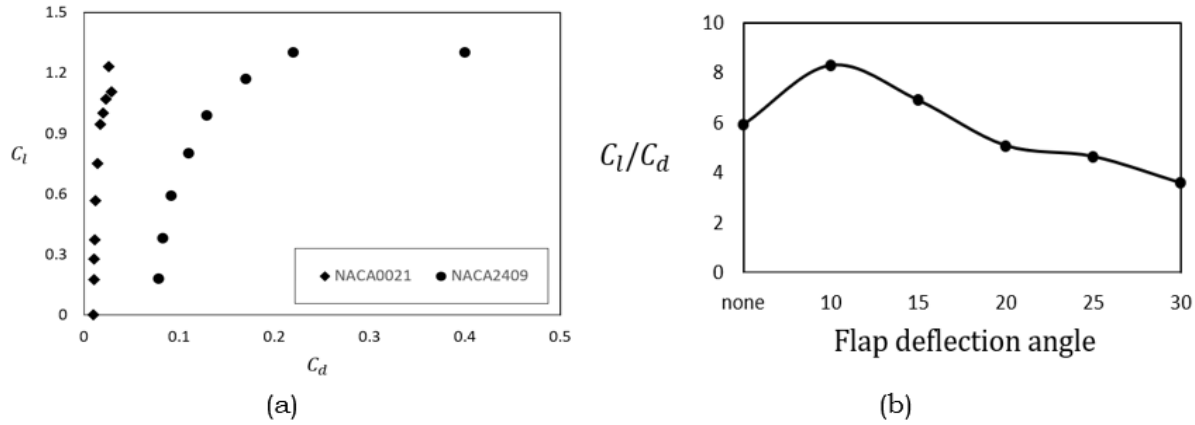

Figure 3-3. The value of (a) lift and drag characteristic of NACA0021 and NACA2409 (b) lift-to-drag ratio of flapped-NACA2409 on particular flap deflection angle

3.3. Vortex Development

One important of aerodynamics analysis is the separated flow characteristics encountered on airfoil bodies. The depth of understanding of the physical flow leads to the prediction of aerodynamics characteristic optimization. The vortex development and stall phenomena related to the separated flow are investigated. This behavior is captured adequately by using numerical simulation as it considers the turbulence model.

The aerodynamics characteristic of airfoil on high α illustrated in Figure 3-4(a), whereby the value of α is adjusted to 10° -15°. The critical angles were found at α =14° and 15° in NACA2409 and NACA0021, respectively. At the critical angle, the value of C_l was suddenly dropped while the value of C_d rapidly grew (Figure 3-4(b)). Detailed physical phenomena of flow patterns and structures developed during a stall, including vortex development, are indicated in the instantaneous streamline (Figure 3-5). It was observable that the vortex shedding was generated at the rear of the airfoil. At the higher α, a large scale of flow separation on the airfoil surface became more unstable, while flow separation was observed after the critical stall angle.

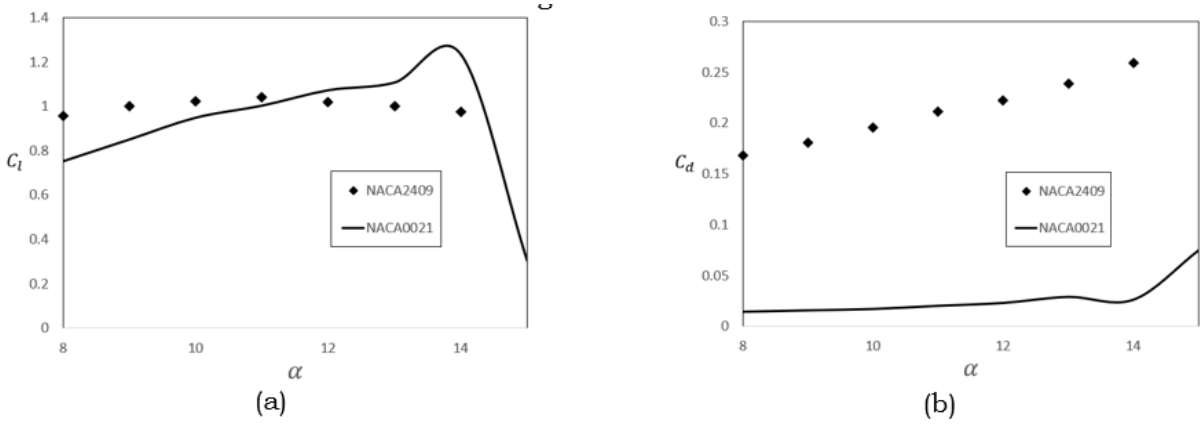

Figure 3-4. The value of (a) C_l and (b) C_d at high α

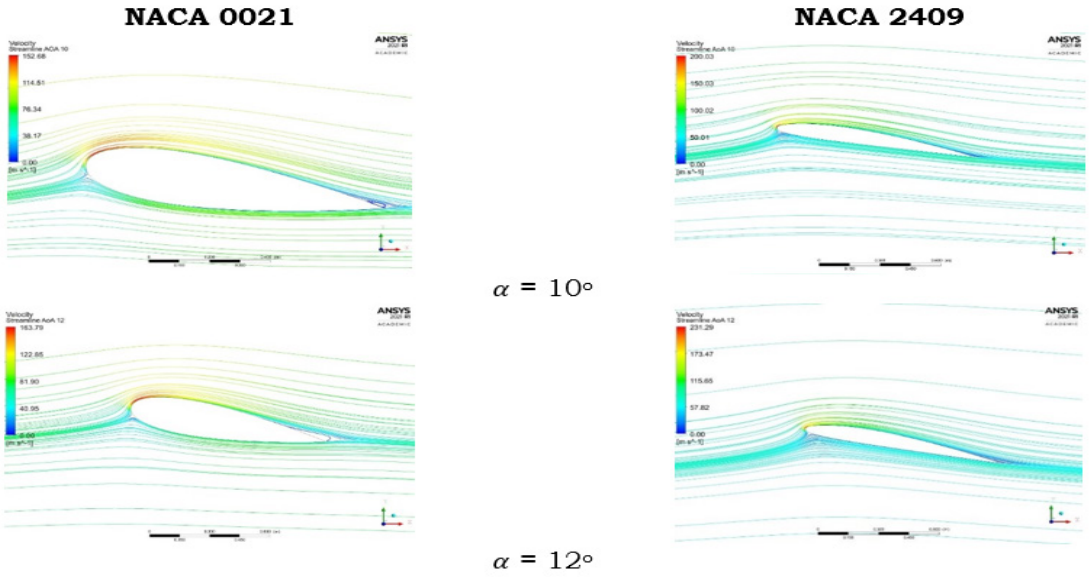

Figure 3-5. Airflow streamline at high α

Next, we observe the fluid flow pattern over the airfoil in a certain α. The flow patterns and aerodynamic characteristics in the NACA 0021 airfoil are given in Figure 3-6. It shows that stagnation streamline is recognized at α = 6°. The flow is attached to the airfoil, whereby the C_l Increases within the range of α = 2° to 12°. The flow over airfoil bodies is on a laminar flow that produces more forces which maximum lift is found at α = 12°. Initial air separation found at α = 8°. After reaching maximum lift, the fluid flow is developed to the unsteady region of stalled. The lift coefficient is rapidly decreasing where the drag coefficient is growing up. Moreover, we also observe the flow pattern of NACA 2409 (Figure 3-7). Compared to the NACA 0021, the flow attached emerges at α = 2° to 12°, which reaches a maximum value at α = 12° where the initial air separation is observed. The initial separation attains at higher than NACA0021. It shows that NACA2409 is more stable than NACA0021 due to the delayed air separation occurrence at higher α.

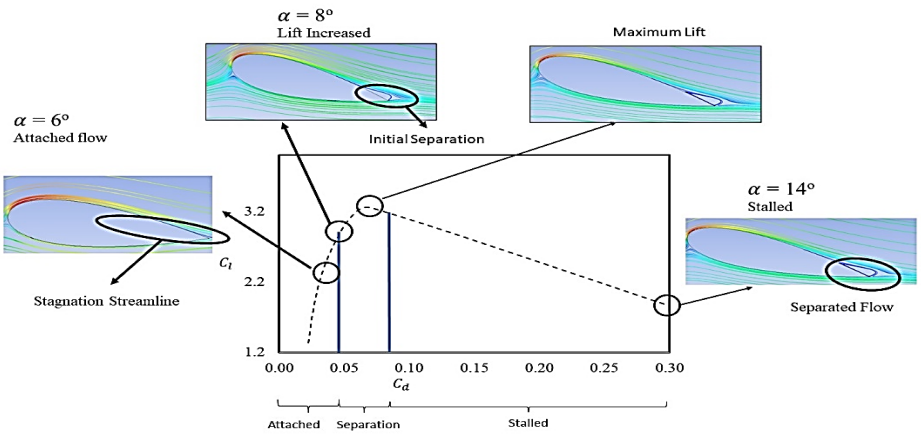

Figure 3-6. The flow region of NACA 0021

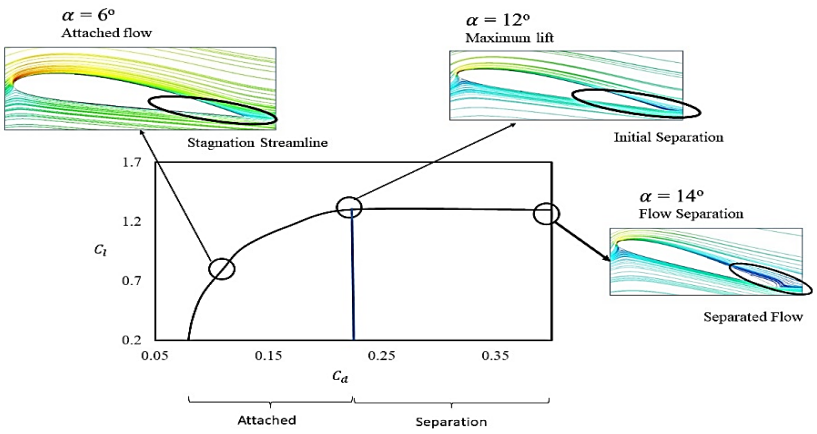

Figure 3-7. The flow region of NACA 2409

The simulation result of flow characteristics shown in Figure 3-8 describes that flap addition removes the leading-edge vortex. The flap deflection angle is greatly influenced the aerodynamics characteristic. From the results, the leading-edge vortex repeatedly emerges at a higher than 15° flap deflection model. This is because the flap deflection angle is too narrow, so the airflow over the upper bodies is separated, leading to airfoil imbalance. Once the leading-edge vortex emerges, the wake of the airfoil exhibits the Von Karman vortex shedding represented by bluff-body separation (Hudy and Naguib, 2006). These are bought to the increase of drag force and loss of lift force all of sudden. The occurred phenomena led to the stall formation. Moreover, the flow region's characteristics on varied angle deflection of flapped-airfoil are also observed in Figure 10. It reveals the cause of lift-to-drag ratio reduction with respect to increasing the flap deflection angle. With the increasing deflection angle, the pressure on the upper airfoil surface is higher than on the lower deflection angle. The air on the upper airfoil boundary remains laminar for low $\alpha\alpha$. It increases the lift coefficient while keeping the drag forces low significantly. On the other hand, at higher α α air separation, the model is more intricate, while the vortex on the flapping tail made the airfoil remains unstable. The maximum lift is obtained at the $\alpha\alpha$ = 12° where an airflow over the upper boundary is on the laminar state. The sudden change of lift and drag occurred at 30° as the stall emerged. It is noticeable that increasing the flap angle shifted the airflow at the upper surface to be more intricate, hence reducing the lift-to-drag ratio. It concludes that flap deflections higher than 10° produce more drag force and unstable conditions whereby the vortex is highly formed.

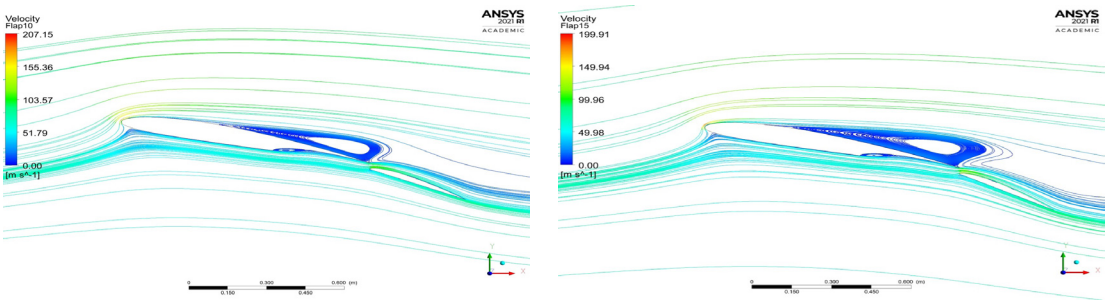

(a) (b)

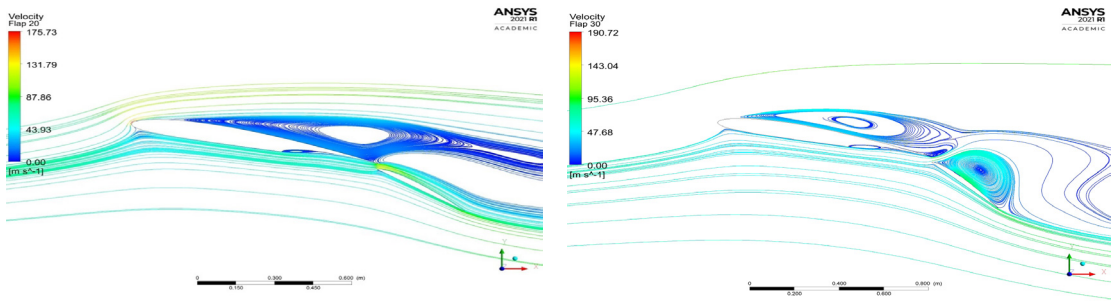

(c) (d)

Figure 3-8. Streamline profile of Flapped-NACA2409 airfoil at flap deflection angle of (a) 10° (b) 15° (c) 20° (d) 30°

4. Conclusion

Detailed steps on the simulation of the airfoil are explained in this work. Based on the observed method, the numerical investigation of the aerodynamic characteristics of airfoils has been done. The employed S-A turbulent model has been able to simulate the aerodynamics characteristic of the airfoil accurately. A parametric study of angle-of-attack is also carried out in order to investigate the optimum performance of airfoil. Several important results and findings are summarized as follows:

1. The validation between numerical and experimental results is performed for standard airfoils without flap addition and obtains good and reasonable accuracy.
2. The boundary layer separation of vortex development and air separation was clearly captured in this simulation. In a standard symmetric airfoil, the vortex shedding regimes begin at α of 8° while the critical angle of stall formation is around 14°. In the NACA2409, initial separation is revealed at higher α than symmetrical airfoil. The airflow behavior is also considered more stable, which yields a higher coefficient of lift than the symmetric airfoil.
3. Flap addition is exposed to increase the value of the lift coefficient on the airfoil. It is evident that flap addition can escalate the C_lC_l by up to 54%, which affected the increase of the value of the lift-to-drag ratio. The optimum airfoil performance with flap addition is investigated by varying the flap deflection angle. It is found that the maximum configuration is obtained on the NACA2409 at α = 12° combined with Fowler flap at 10° deflection angle. The parametric study in the whole range of parameters leads to satisfactory results. This result strengthens the robustness of the S-A turbulence model and projects the use of the S-A model for dealing with aerodynamics analysis. It can be concluded that this model is suitable for simulating the aerodynamic phenomena on the two-dimensional airfoil.

Acknowledgments

We acknowledge a collaborative funding program from the Institution of Research and Community Service (LPPM) Institut Teknologi Dirgantara Adisutjipto. The author would like to thank Dr. Prasetyo Edi and Dr. Muhammad Ridlo Erdata Nasution for the discussion.

Contributorship Statement

OD is the main contributor to this research by developing the concept and supervising the manuscript, BJ and MH conduct the simulations and analyze the results, and TW proofreads the writing and suggests improvements.

References

Ahmed, M.R., Sharma, S. D. An investigation on the aerodynamics of a symmetrical airfoil in ground effect, 2005. Exp. Therm. Fluid Sci., vol. 29, no. 6, pp. 633–647.

Andersson, B., Andersson, R., Håkansson, L., Mortensen, M., Sudiyo, R., & Van Wachem, B., 2011. Computational Fluid Dynamics for Engineers. Cambridge University Press.

Andrea C, Valerio D, Francesco B. A Spalart-Allmaras turbulence model implementation in a discontinuous Galerkin solver for incompressible flows. 2013. *J.Comput.Phys*. Volume 241. Pages 388-415.

ANSYS Fluent documentation, theory guide, 2016

Brunton, S.L. (2022). Applying Machine Learning To Study Fluid Mechanics. Acta Mech. Sin.

Casey, M., Wintergerste, T., 2000. ERCOFTAC Special Interest Group on "Quality and Trust in Industrial CFD, Best Practice Guidelines. ERCOFTAC.

Crivellini, A., D'Alessandro, V. Spalart–Allmaras model apparent transition and RANS simulations of laminar separation bubbles on airfoils, 2014, *International Journal of Heat and Fluid Flow*, Volume 47, Pages 70-83.

Duraisamy, K., Iaccarino, G., Xiao, H. (2019). Turbulence Modeling In The Age Of Data. Annual Review Of Fluid Mechanics, 51:1, 357-377

Gregorek, G.M., Hoffmann, M.J., Berchak, M.J. 1989, Steady State and Oscillatory Aerodynamic Characteristics of a NACA 0021 Airfoil: Data Report. Ohio State University, Columbus, OH.

Hudy, L. M., Naguib, A., and Humphreys, W. M., 2007, "Stochastic Estimation of the Separation-Flow Field Using Wall-Pressure-Array Measurements," Physic of Fluids. Volume 19, p. 024103.

Kay, N.J., Richards, P.J., harma, R.N. 2020. Influence of Turbulence on Cambered and Symmetrical Airfoils at Low Reynolds Numbers, *AIAA Journal*, vol 58, Pages 1913-1925.

Li, Y. Wang, J., Zhang, P. 2002. Effects of Gurney flaps on a NACA0012 airfoil," *Flow, Turbul. Combust.,* vol. 68, no. 1, pp. 27–39.

Rao, T.S., Mahapatra, T., Mangavelli, S.C. 2018. Enhancement of Lift-Drag characteristics of NACA 0012. *Mater. Today Proc.*, vol. 5, no. 2, pp. 5328–5337.

Rhee, S.H., Kim, S.E., Ahn, H., Oh, J., Kim, H. 2003. Analysis of a jet-controlled high-lift hydrofoil with a flap, Ocean Eng., vol. 30, no. 16, Pages. 2117–2136.

Rocha, P.A., Roch, H.H.B., Carneiro, F.O., da Silva. M.E.V., de Andrade, C.D., 2016 .A case study on the calibration of the k–ω SST (shear stress transport) turbulence model for small scale wind turbines designed with cambered and symmetrical airfoils. *Energy*, volume 97. pp. 144-150

Rostamzadeh, N., Kelso, R.M., Dally, B.B., Hansen, K.L. 2013. The effect of undulating leading-edge modifications on NACA 0021 airfoil characteristics, *Phys. Fluids*, vol. 25, 117101.

Shukla, V., Kaviti, A.K. 2017. Performance evaluation of profile modifications on

straight-bladed vertical axis wind turbine by energy and Spalart Allmaras models. *Energy*, Volume 126, Pages 766-795,

Spalart, P., Allmaras, S. 1992. A one-equation turbulent model for aerodynamic flows. AIAA 1992-439. *30th Aerospace Sciences Meeting and Exhibit*.

Torres, G. E., and Mueller, T. J., 2004. Aerodynamic Characteristics of Low Aspect Ratio Wings at Low Reynolds Numbers. *AIAA Journal*, Vol 42:5, Pages 865-873.

Wang, W., Lie, P., Tian, Y., Qu, Q. 2015. Numerical Study of the Aerodynamic Characteristics of High-Lift Droop Nose with Deflection of Fowler Flap and Spoiler. *Aerospace Science and Technology*. Voume 48, Pages 75-85.

Wendt, J., 2008. Computational fluid dynamics: an introduction, Springer.

Windte, J., Scholz U, Radespiel R. 2006. Validation of the rans-simulation of laminar separation bubbles on airfoils. *Aerosp Sci Technol.* Volume 10, Pages 484-494.

Wolfe, W.P, Ochs, S.S. 1997. Predicting Aerodynamics Characteristic of Typical Wind Turbine Airfoils Using CFD. *Sandia National Laboratories Report*.